Dielectric relaxation of isotactic polystyrene above the glass transition temperature

Koji Fukao* and Yoshihisa Miyamoto
Department of Physics, College of Liberal Arts and Sciences, Kyoto University, Kyoto 606, Japan
(Received 2 March 1992; revised 23 March 1992)

The α-relaxation was investigated by dielectric measurements in isotactic polystyrene crystallized isothermally for various crystallization times at crystallization temperatures from 423 to 483 K. The thickness of the amorphous layer in crystallized samples, determined by small-angle X-ray scattering, increases with increasing crystallization temperature. The relaxation time obeys the Williams–Landel–Ferry equation and increases with increasing crystallinity and with decreasing crystallization temperature. The decay function was calculated directly from the dielectric loss. The decay function shows a crossover from a stretched-exponential decay (the Williams–Watts equation) to a power-law decay (t^{-n}) as the relaxation proceeds. The exponent n of the power-law decay increases with decreasing crystallinity and with increasing crystallization temperature.

(Keywords: isotactic polystyrene; crystallinity; crystallization temperature; dielectric relaxation; decay function; power-law decay)

INTRODUCTION

Semicrystalline polymers show primary relaxations (α-relaxations) which are due to the segmental motion of polymer chains in amorphous layers intervening between crystalline lamellae[1]. It is known that the relaxation behaviours of semicrystalline polymers are quite different from those of amorphous polymers. In amorphous polymers, the shape of the dielectric loss curve *versus* frequency does not change with temperature and the time–temperature superposition law is valid. In poly(vinylidene fluoride), however, the width of the dielectric loss profile in frequency domain increases with decreasing temperature and the time–temperature superposition law does not hold[2]. In poly(ethylene terephthalate) (PET), the shape of the dielectric loss curve *versus* frequency broadens as crystallinity increases[3,4]. These properties are usually thought to be associated with the constraint of polymer chains in amorphous layers caused by the existence of crystalline layers. In other words, the number of loops, tie molecules and cilia[5], the randomness near the interface between amorphous layers and crystalline layers[6], and/or the thickness of amorphous layers[7] affect the dielectric relaxation behaviours of polymer chains in amorphous layers. These quantities are changed by higher-order structures of polymer crystals or by the crystallization conditions. Hence, it is important to use samples crystallized under well-controlled conditions in order to elucidate the relation between the dielectric behaviours and the structure of amorphous layers.

In this paper, we investigate the α-relaxations of isotactic polystyrene (iPS) with various crystallinities and thicknesses of amorphous layers, crystallized isothermally by controlling the crystallization conditions. The change in dielectric behaviours with crystallinity has been reported in many crystalline polymers, but little attention has been paid to the change with crystallization temperature except for PET. Saito[8] investigated the dielectric relaxation behaviours of PET and reported that the α-relaxation depends not only on crystallinity but also on crystallization temperature.

The purpose of the present paper is to investigate the dependence of the α-relaxation of iPS on the crystallization conditions by using dielectric measurements and small-angle X-ray scattering (SAXS) and to clarify the mechanism of the α-relaxation. We obtain the decay function directly from the dielectric loss obtained experimentally in the same way as in ref. 9 and examine the change in the decay function with crystallinities and thicknesses of amorphous layers.

EXPERIMENTAL

Sample preparation

The polymer used in this study was purchased from Polymer Laboratories Ltd. The weight-average molecular weight M_w was 5.56×10^5 and M_w/M_n was 1.9 (where M_n is the number-average molecular weight). The powder sample was melted *in vacuo* at 553–563 K and cooled to room temperature by circulating water to obtain a plate-like sample of about 0.1 mm thickness (iPS-1). It was confirmed by wide-angle X-ray scattering that the diffraction patterns of iPS-1 have only amorphous haloes and this sample has no crystalline component. Hence the amorphous phase of iPS-1 is free from the constraint imposed by the crystalline phase. We refer to this

* To whom correspondence should be addressed

0032-3861/93/020238-09

Table 1 Crystallization temperatures, density and crystallinity

	T_c (K)	ρ (g cm^{-3}) As prepared	ρ (g cm^{-3}) After measurements	χ (%)[a]
Type I				
iPS-1	–	1.0580	1.0597	1.3
iPS-2	448	1.0590	1.0615	3.3
iPS-3	448	1.0622	1.0626	6.5
iPS-4	449	1.0672	1.0684	14.5
iPS-5	450	1.0743	1.0751	24.5
iPS-6	449	1.0761	1.0769	27.0
Type II				
iPS-7	423	1.0739	1.0737	23.2
iPS-8	449	1.0761	1.0769	27.0
iPS-9	463	1.0765	1.0770	27.4
iPS-10	473	1.0767	1.0780	28.3
iPS-11	483	1.0773	1.0771	28.0

[a] Crystallinity χ is calculated by using averaged densities of before and after measurements

amorphous phase as isotropic amorphous phase. Other samples were prepared by heating amorphous plates obtained in the way described above *in vacuo* at 553–563 K, cooling down to crystallization temperature (T_c) under nitrogen atmosphere and crystallizing them isothermally at T_c. Two types of samples were prepared as listed in *Table 1*. Type I samples (from iPS-2 to iPS-6) were crystallized at 449 K (±1 K) and their crystallinities changed from 3 to 27% with increasing crystallization time. Type II samples (from iPS-7 to iPS-11) were crystallized at other values of T_c long enough for the crystallization process to be completed. Density was measured at 298 K in a density gradient column. The crystallinity χ was determined from the density ρ by the relation:

$$\chi = \rho_c(\rho - \rho_a)/\rho(\rho_c - \rho_a)$$

where ρ_c and ρ_a are the densities of crystalline and amorphous parts, respectively. A value of 1.13 g cm^{-3} was adopted for ρ_c[10,11] and the density of iPS-1 as prepared was taken as ρ_a. Observation by optical microscope showed that iPS-1 had no optical anisotropy. As crystallinity increased or crystallization time elapsed, spherulites appeared in isotropic amorphous phases and grew until the sample was quenched to room temperature or filled with spherulites.

Small-angle X-ray scattering

SAXS measurements were carried out at the High Intensity X-ray Laboratory (HIXLAB) of Kyoto University. The X-ray source was CuK_α from a fine-focus X-ray generator (RU-1000, Rigaku Corporation). The X-ray intensities were measured by a two-dimensional position-sensitive proportional counter and corrected for the non-uniformity of detector sensitivity and then circularly averaged to obtain the one-dimensional intensity. The sample-to-detector distance was 1640 mm. All SAXS measuresments were made at room temperature.

Dielectric measurements

Dielectric measurements were made using an LCR meter (Hewlett-Packard, HP4284A). Measurements covered the frequency range 100 Hz–1 MHz and the temperature range 300–445 K. Gold was evaporated as electrodes onto the samples. Since the measurements were made mainly above the glass transition temperature ($T_g \approx 363$ K), we measured the densities after measurements to check the degree of crystallization during the measurements. The densities before and after the measurements are listed in *Table 1*. The variations in crystallinities during measurements were small and are shown as error bars in the figures.

RESULTS AND DISCUSSION

SAXS measurements

Figure 1 shows an example of one-dimensional SAXS profiles $I(q)$ for crystallized iPS, where $q = 4\pi \sin\theta/\lambda$ is the magnitude of the scattering vector, 2θ is the scattering angle and λ is the X-ray wavelength. For all samples of iPS the plots of $I(q)q^4$ *versus* q^4 resulted in straight lines at larger scattering angles.This indicates a scattering law $I(q) = \xi_1 q^{-4} + \xi_2$, where ξ_2 is the intensity of the fluid-like scattering related to the content of amorphous material. The values of ξ_2 obtained from the plots were used as the intensity of background scattering. Fully crystallized samples of iPS (iPS-6 and type II samples) consist of stacks of lamellae, showing electron density variations in only one direction. Since the distribution of such stacks in the samples is isotropic, we obtain the one-dimensional correlation function $\gamma(r)$ from the relation:

$$\gamma(r) = \int_0^\infty q^2\tilde{I}(q)\cos(qr)\,dq \Big/ \int_0^\infty q^2\tilde{I}(q)\,dq \qquad (1)$$

where $\tilde{I}(q)$ is the scattering intensity corrected for background. Experimental one-dimensional correlation functions were evaluated by equation (1) as shown in *Figure 2*. Long spacing L, crystalline thickness l_c and amorphous thickness l_a were determined for iPS with various values of T_c according to the procedure given by Strobl and Schneider[12] (*Table 2*). It is found that both long spacing and amorphous thickness increase with increasing T_c.

Dielectric measurements

Temperature dependences of dielectric constant ε' and dielectric loss ε'' are shown in *Figure 3* for iPS-6, whose crystallinity χ is 27%. The α-relaxation due to the

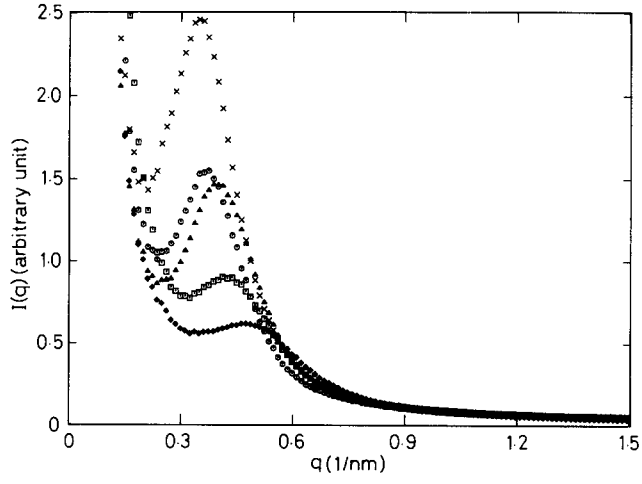

Figure 1 SAXS profiles for samples of type II: ◇, iPS-7; □, iPS-8; △, iPS-9; ○, iPS-10; ×, iPS-11

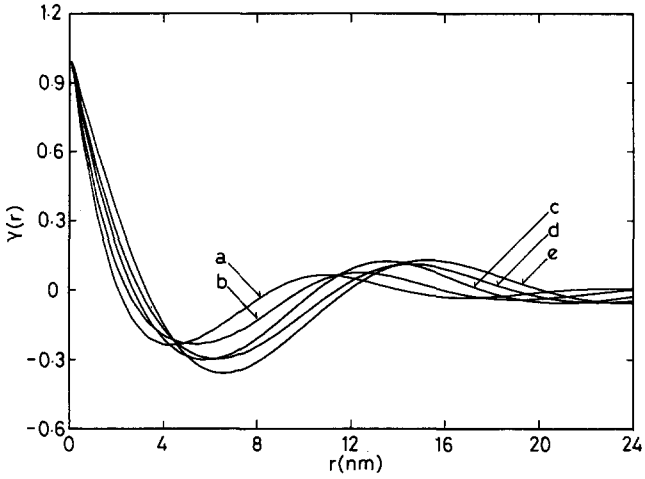

Figure 2 Experimental correlation functions $\gamma(r)$ obtained for the samples of type II: a, iPS-7; b, iPS-8; c, iPS-9; d, iPS-10; e, iPS-11

Table 2 Dependence of L, l_c and l_a on T_c

	T_c (K)	L (nm)	l_c (nm)	l_a (nm)
iPS-7	423	11.0	2.0	9.0
iPS-8	449	12.4	2.3	10.1
iPS-9	463	13.6	3.0	10.6
iPS-10	473	14.5	3.2	11.3
iPS-11	483	15.3	4.1	11.2

segmental motion of polymer chains in amorphous phases is observed above T_g and the peak positions of ε'' are shifted to higher temperature with increasing frequency. Other relaxations, however, are not observed within the experimental accuracy in the present temperature range. These results agree with those of Yano and Wada[13]. They have not observed the β-relaxation in iPS.

Figure 4 shows examples of frequency dependences of ε' and ε'' at various temperatures for type I samples. It is found that the peak height of dielectric loss curves increases with increasing temperature and with decreasing crystallinity. The loss curves at various temperatures can be reduced to a master curve, as shown in *Figure 5*, by using the peak position f_{max} and peak value ε''_{max}. Since the master curves exist for each sample, the temperature change in the shape of the dielectric loss curve can be neglected within the present temperature range. The shape of reduced loss curves is broader than that of the Debye relaxation and is asymmetric. In order to evaluate the broadness and asymmetry of dielectric loss curves, the reduced experimental data in *Figure 5* are fitted by the Havriliak–Negami (HN) equation[14]:

$$\frac{\varepsilon^*(\omega) - \varepsilon_\infty}{\varepsilon_0 - \varepsilon_\infty} = [1 + (\omega\tau_0)^{1-\tilde{\alpha}}]^{-\tilde{\beta}} \qquad (2)$$

where ω is angular frequency, ε^* is complex dielectric constant ($\varepsilon^* = \varepsilon' - i\varepsilon''$), $1 - \tilde{\alpha}$ is the width parameter, $\tilde{\beta}$ is the skewness parameter, τ_0 is the central relaxation time, ε_0 and ε_∞ are the limiting low- and high-frequency dielectric permittivities, respectively. The parameters obtained are listed in *Table 3*. The values of $1 - \tilde{\alpha}$ and $-(1 - \tilde{\alpha})\tilde{\beta}$ represent slopes of dielectric loss curves in low and high frequency ranges, respectively. For type I samples it is found that the absolute values of slope in the low frequency side are larger than those in the high frequency side, and the slope in the high frequency side does not change with crystallinity while the slope in the low frequency side decreases with increasing crystallinity. For type II samples, the shape of dielectric loss curves changes with T_c. The slope in the high frequency range does not change, while the slope in the low frequency range increases with increasing T_c.

The temperature dependences of f_{max}, which corresponds to the reciprocal of relaxation time, are shown in *Figures 6* and *7*. *Figure 6* shows that at a constant temperature the relaxation time increases with increasing crystallinity. The increase in crystallinity at constant T_c means an increase in spherulite fraction relative to the isotropic amorphous phase. Hence, it follows that the increase in spherulite fraction leads to the slowing down of the α-relaxation process. For type II, f_{max} at a constant temperature increases slightly as T_c increases. The values of f_{max} for these two types of sample can be well reproduced in terms of the Williams–Landel–Ferry (WLF) equation[15], described by:

$$f_{max} = f_0 \exp\left[\frac{C_1(T - T_0)}{C_2 + (T - T_0)}\right] \qquad (3)$$

where $C_1 = 8.86$, $C_2 = 101.6$ K, f_0 and T_0 are fitting parameters. The fitted values of f_0 and T_0 are listed in *Table 3*. The value of T_0 is about 400 K for all samples. *Figure 8* shows the reduced values of f_{max} as a function of $T - T_0$. All the data are on the WLF master curve regardless of crystallinity and T_c.

The dielectric strength $\Delta\varepsilon$ ($=\varepsilon_0 - \varepsilon_\infty$) is obtained by multiplying $\Delta\varepsilon/\varepsilon''_{max}$ in *Table 3* by $\varepsilon''_{max}(T)$. *Figure 9* shows the temperature dependence of $T\Delta\varepsilon$ for type I. The

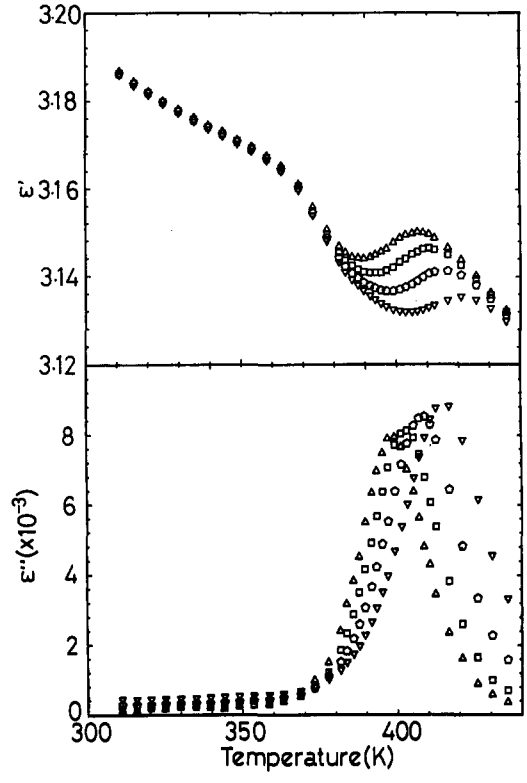

Figure 3 Temperature dependence of dielectric constant (ε') and dielectric loss (ε'') of iPS-6: △, 400 Hz; □, 1000 Hz; , 3000 Hz; ▽, 10000 Hz

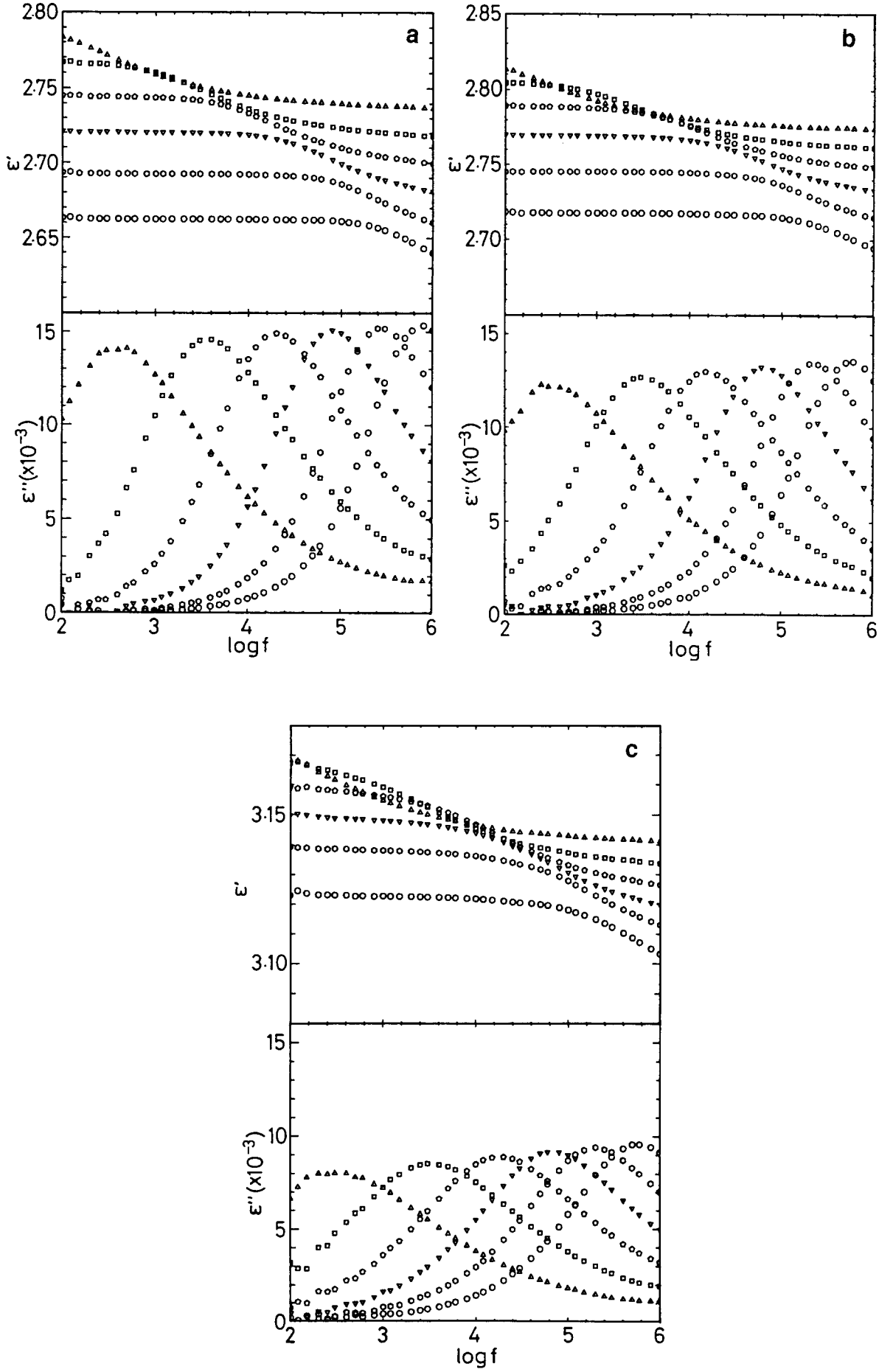

Figure 4 Dependence of ε' and ε'' on the logarithm of frequency (Hz) at various temperatures. (a) iPS-1: △, 391.4 K; □, 401.7 K; ⬠, 411.0 K; ▽, 420.4 K; , 429.9 K; ○, 439.7 K. (b) iPS-3: △, 391.9 K; □, 401.6 K; ⬠, 410.8 K; ▽, 420.5 K; ⬡, 430.0 K; ○, 439.2 K. (c) iPS-6: △, 394.2 K; □, 404.7 K; ⬠, 414.9 K; ▽, 424.8 K; ⬡, 434.1 K; ○, 444.7 K

dielectric strength would be proportional to $1/T$, that is, $T\Delta\varepsilon$ is constant, if there were no correlation among the segments. However, it is found in *Figure 9* that $T\Delta\varepsilon$ increases with temperature, i.e. correlation exists between the segments.

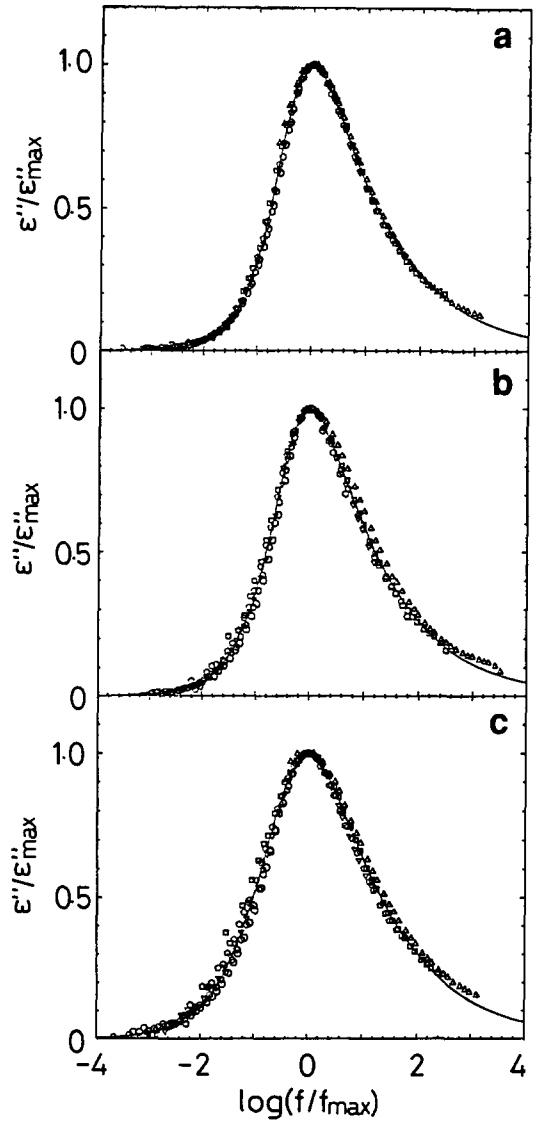

Figure 5 Dependence of reduced dielectric loss ($\varepsilon''/\varepsilon''_{max}$) on the logarithm of reduced frequency (f/f_{max}). (a) iPS-1; (b) iPS-3; (c) iPS-6. The symbols are the same as in *Figure 4*. The solid lines are given by the HN equation

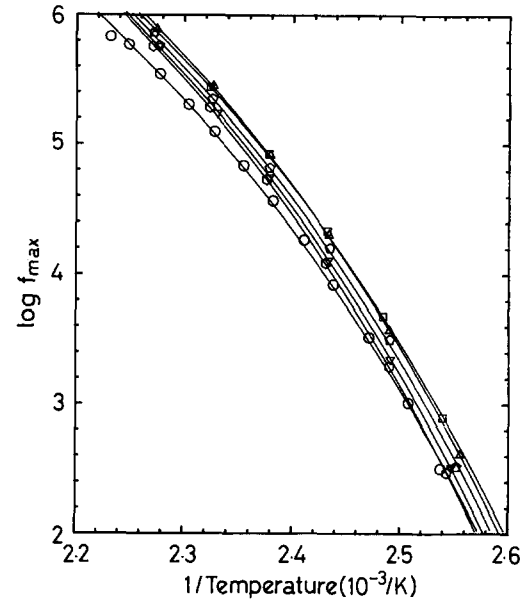

Figure 6 Arrhenius plot of the logarithm of f_{max} (Hz) with temperature for samples of type I: △, iPS-1; □, iPS-2; ⬠, iPS-3; ▽, iPS-4; ⬡, iPS-5; ○, iPS-6. The solid lines are given by the WLF equation

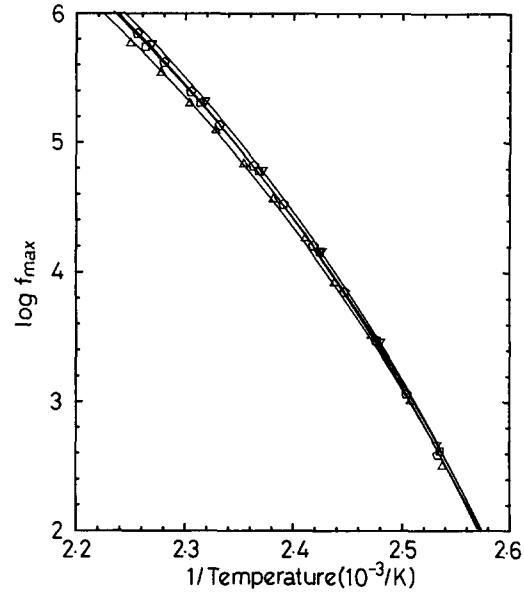

Figure 7 Arrhenius plot of the logarithm of f_{max} (Hz) with temperature for samples of type II: △, iPS-8; □, iPS-9; ⬠, iPS-10; ▽, iPS-11. The solid lines are given by the WLF equation

Table 3 List of fitting parameters

			HN equation			WLF equation	
	T_c (K)	χ (%)	$1-\tilde{\alpha}$	$-(1-\tilde{\alpha})\tilde{\beta}$	$\Delta\varepsilon/\varepsilon''_{max}$	f_0 (10^3 Hz)	T_0 (K)
Type I							
iPS-1	–	1.3	0.962	−0.359	3.53	2.6	400
iPS-2	448	3.3	0.923	−0.387	3.46	2.0	398
iPS-3	448	6.5	0.901	−0.373	3.58	2.1	400
iPS-4	449	14.5	0.795	−0.333	4.10	2.2	401
iPS-5	450	24.5	0.745	−0.359	4.12	2.3	402
iPS-6	449	27.0	0.735	−0.355	4.17	1.1	399
Type II							
iPS-7	423	23.2	0.724	−0.364	4.18	1.9	402
iPS-8	449	27.0	0.735	−0.355	4.17	1.2	400
iPS-9	463	27.4	0.748	−0.382	3.98	1.6	401
iPS-10	473	28.3	0.747	−0.362	4.07	1.9	402
iPS-11	483	28.0	0.758	−0.355	4.09	2.1	402

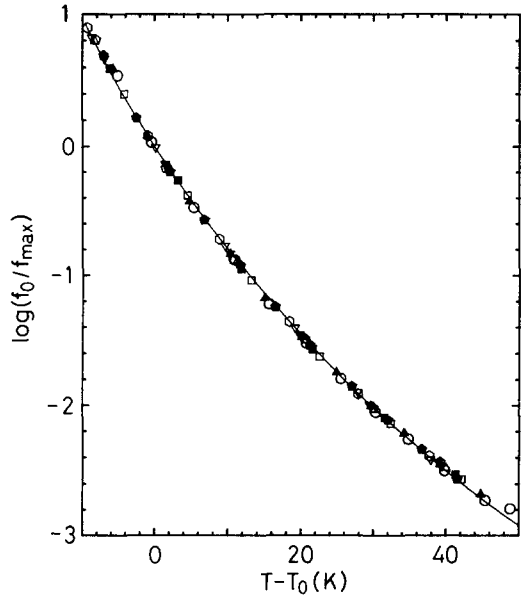

Figure 8 Logarithm of f_0/f_{max} *versus* $T - T_0$. The values of T_0 and f_0 are listed in *Table 2*. △, iPS-1; □, iPS-2; ⬡, iPS-3; ▽, iPS-4; ⬡, iPS-5; ○, iPS-6; ▲, iPS-8; ■, iPS-9; ⬢, iPS-10; ▼, iPS-11. The solid line is given by the WLF equation

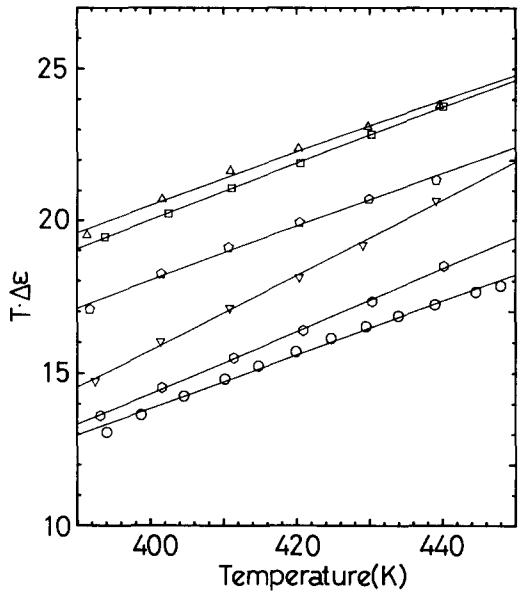

Figure 9 Dependence of $T\Delta\varepsilon$ on temperature for samples of type I. The solid lines are reproduced by the two-site model. The symbols are the same as in *Figure 6*

Figure 10 shows the dependence of dielectric strength on crystallinity at 411 K for type I samples. The values of $\Delta\varepsilon$ for $\chi \geqslant 10\%$ decrease linearly with increasing crystallinity. This straight line crosses the horizontal axis when χ is 100%. This behaviour is consistent with the fact that the α-relaxation of iPS is associated with the motion of amorphous chains. However, the values of $\Delta\varepsilon$ for $\chi \leqslant 10\%$ are not on this straight line and deviate above the line. This behaviour is observed not only in iPS but also in other crystalline polymers such as PET[4] and copolymers of adipic acid with 1,6- and 2,5-hexanediols[16].

Decay function

In the previous section we have discussed the shape of dielectric loss *versus* frequency by using the HN equation. The dielectric loss could be reproduced sufficiently by this equation and the characteristic features of the shape of α-relaxation are given by the fitting parameters $\tilde{\alpha}$ and $\tilde{\beta}$. The relationship between the parameters and the physical process underlying the α-relaxation, however, is still unclear. Here we obtain decay functions $\phi(t)$ directly from the experimental dielectric losses in order to elucidate the physical process. The decay function, i.e. the dipole autocorrelation function, is related to dielectric loss by [17]:

$$\phi(t) = \frac{2}{\pi}\int_0^\infty \frac{\varepsilon''(\omega)}{\varepsilon_0 - \varepsilon_\infty}\cos\omega t\,\frac{d\omega}{\omega} \qquad (4)$$

For the α-relaxation of iPS, we can use the reduced dielectric loss curves as a function of reduced frequency in *Figure 5* in order to obtain the dielectric decay function, because the time–temperature superposition law is valid in this case (see Appendix). The calculated values of $\phi(t)$ are shown in *Figure 11a* for type I samples, where the relaxation time τ is defined as $\phi(\tau) = e^{-1}$. We have confirmed that τ is almost equal to the reciprocal of f_{max} and has the same dependence on χ and T_c as f_{max}^{-1} does. In *Figure 11a* we find that the overall behaviours can be fitted by the Williams–Watts (WW) equation[18]:

$$\phi(t) = \exp[-(t/\tau)^\beta]$$

for all crystallinities. The values of β_{WW}, which is a fitting parameter β obtained by fitting the decay function throughout all decades with the WW equation, discontinuously change near $\chi \approx 10\%$ for type I; $\beta_{WW} \approx 0.41$ for $\chi \geqslant 10\%$ while $\beta_{WW} \approx 0.47$ for $\chi \leqslant 10\%$. For type II the values of β_{WW} are almost constant (≈ 0.41). In *Figure 11b*, however, it is clear that a power-law decay region exists at long times and the relaxation in this region becomes slower as crystallinity increases.

Here we introduce the relaxation rate $k(t) = -\dot{\phi}(t)/\phi(t)$ in order to investigate the change in relaxation behaviours. If $k(t) \propto t^{\beta-1}$ $(0 \leqslant \beta < 1)$, we obtain the decay function as follows:

$$\phi(t) = \begin{cases} \exp[-(t/\tau)^\beta] & (0 < \beta < 1) \\ \phi_0 t^{-n} & (\beta = 0) \end{cases} \qquad (5)$$

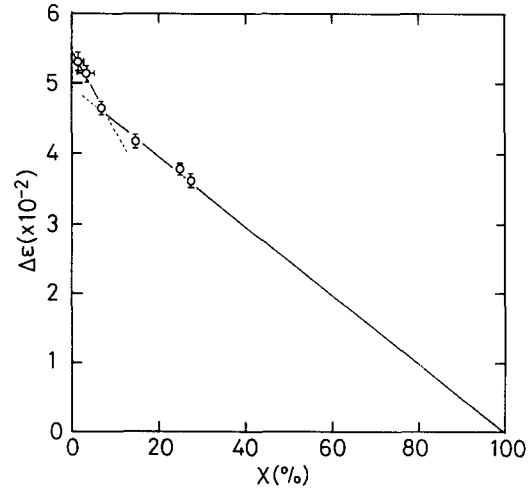

Figure 10 Dependence of dielectric strength ($\Delta\varepsilon$) on crystallinity χ at 411 K for samples of type I. Horizontal error bars show the change in χ during measurements and vertical error bars show the variation in thickness of the samples

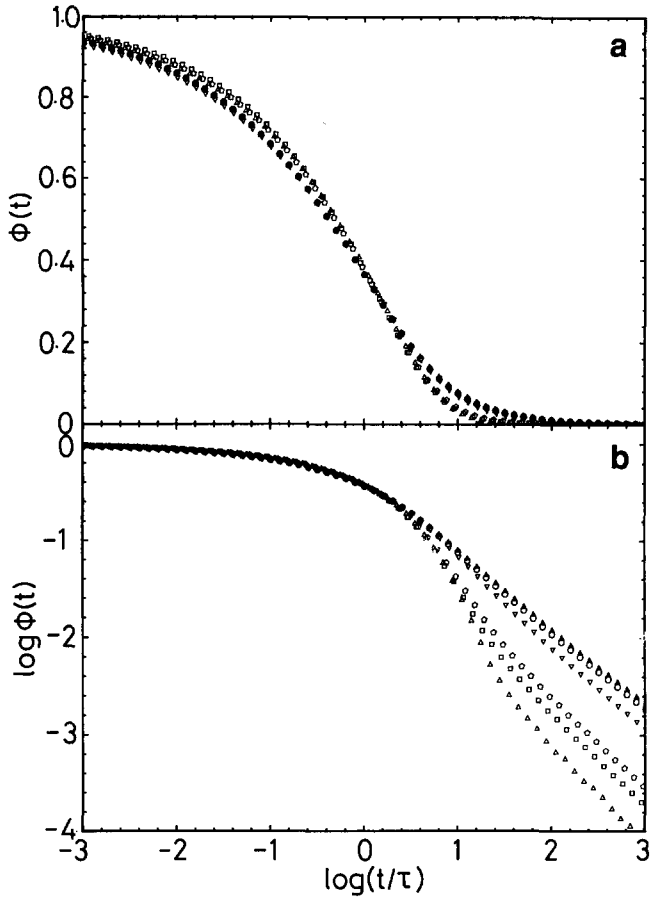

Figure 11 Dependence of decay function on reduced time for samples of type I. Vertical axis is on (a) a linear scale and (b) a logarithmic scale. △, iPS-1; □, iPS-2; ⬠, iPS-3; ▽, iPS-4; ○, iPS-5; ▲, iPS-6

where ϕ_0 and n are constants. Therefore we can determine the shape of the decay function by plotting $\log k(t)$ as a function of $\log t$. *Figure 12* shows the reduced rate constant $\tilde{k}(t)(\equiv k(t)\tau$, where τ is independent of time) *versus* $\log t/\tau$. As already reported in ref. 9, it is found that $\tilde{k}(t)$ has three distinct regions (I, II and III) for low crystallinity, while $\tilde{k}(t)$ has only two different regions (I and II) for high crystallinity. As crystallinity increases, the intermediate region III, which exists for low crystallinity, becomes narrow, vanishing at $\chi \approx 15\%$. In the low crystallinity samples the slope of region I is -0.58, while the slope of region II is about -1; these values are the same as those of the high crystallinity samples. It follows that the decay function can be expressed as the WW equation with $\beta = 0.42$ in region I and a power-law equation in region II regardless of crystallinity. Although the value of β in region I is independent of χ, the exponents n of the power-law decay in region II, which can be obtained from *Figure 11b*, depend on crystallinity and they decrease with increasing crystallinity as shown in *Figure 13a*. Relaxation behaviours in regions I and II seem to be strongly connected with each other, while they are not connected with region III. Here we assume that the relaxation mechanism associated with region III is different from that associated with regions I and II. In *Figure 12* we regard the crossing point of the extrapolated straight line of region I with that of region II as a crossover time between regions I and II ($\tilde{t}_1$). As shown clearly in *Figure 12*, the crossover time $\tilde{t}_1$ is shifted to shorter time regions as crystallinity increases. Here it should be noted that a discontinuous change in β_{WW} at $\chi = 10\%$ is due to the existence of region III in lower crystallinity samples.

The results for type II were analysed in the same way as type I. The shape of the decay function of type II shows little difference from that of high crystallinity samples of type I, except that the exponents n of a power-law decay in region II increase with increasing crystallization temperature as shown in *Figure 13b*. In this case, the shift of $\tilde{t}_1$ with T_c could not be observed within the experimental accuracy.

SUMMARY

We have obtained the following results on the α-relaxation of iPS by dielectric measurements and

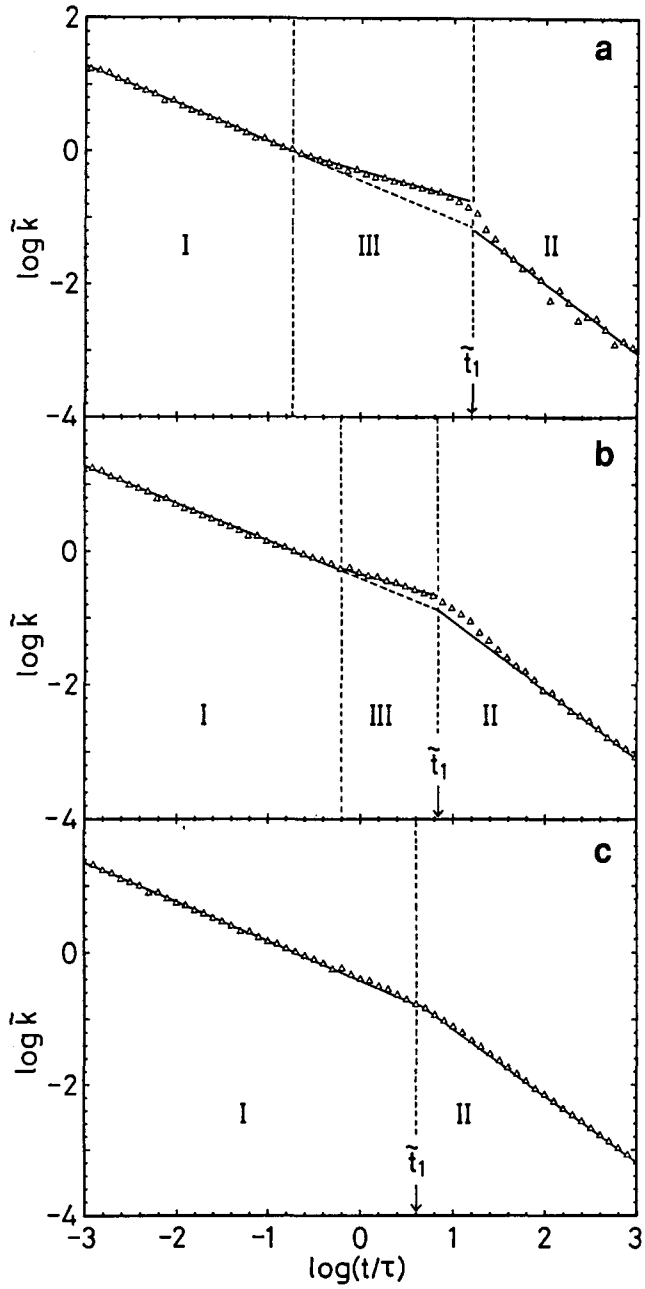

Figure 12 Dependence of reduced rate constant on reduced time: (a) iPS-1; (b) iPS-3; (c) iPS-6

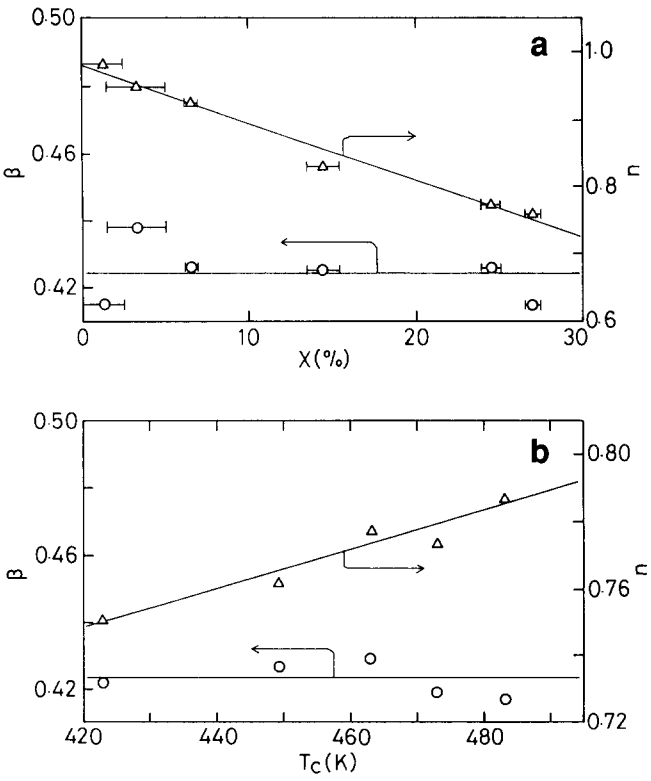

Figure 13 (a) Dependence of β and n on χ for samples of type I. (b) Dependence of β and n on T_c for samples of type II. ○, β; △, n

SAXS. The following results, 1–3, are obtained regardless of crystallinity and T_c.

1. For each sample, dielectric loss curves as a function of log f at various temperatures can be reduced to a single master curve.
2. Temperature dependence of the frequency giving the peak position in dielectric loss *versus* frequency curves obeys the WLF equation.
3. Decay function $\phi(t)$ is of the WW type in the short-time region and shows a crossover to a power-law decay in the long-time region.

For samples of types I and II, results 4 and 5, respectively, were obtained.

4. As crystallinity increases at $T_c \approx 449$ K, the relaxation time τ increases, the exponent of the power-law decay n decreases and the crossover point $\tilde{t}_1$ becomes smaller.
5. As crystallization temperature increases, the thickness of amorphous layers increases, the relaxation time decreases and the exponent of the power-law decay increases.

ACKNOWLEDGEMENTS

The authors express their cordial thanks to Professor H. Miyaji (Kyoto University) for useful discussions and to the committee of HIXLAB of Kyoto University for the use of the 6-m SAXS system. The authors also thank the Ministry of Education, Science and Culture of Japan for a Grant-in-Aid.

REFERENCES

1 McCrum, N. G., Read, B. E. and Williams, G. 'Anelastic and Dielectric Effects in Polymeric Solids', Wiley, New York, 1967
2 Sasabe, H., Saito, S., Asahina, M. and Kakutani, H. *J. Polym. Sci.* 1969, **A27**, 1405
3 Ishida, Y., Yamafuji, K., Itoh, H. and Takayanagi, M. *Kolloid Z. Z. Polym.* 1962, **184**, 97
4 Boyd, R. H. *Polymer* 1985, **26**, 323
5 Mansfield, M. L. *Macromolecules* 1983, **16**, 914
6 Hahn, B. R., Wendorff, J. and Yoon, D. Y. *Macromolecules* 1985, **18**, 718
7 Guttman, C. M., DiMarzio, E. A. and Hoffman, J. D. *Polymer* 1981, **22**, 1466
8 Saito, S. *Res. Electrotech. Lab. (Tokyo)* 1964, no. 648
9 Fukao, K., Miyamoto, Y. and Miyaji, H. *J. Phys. Condens. Matter* 1991, **3**, 5451
10 Natta, G. and Corradini, P. *Makromol. Chem.* 1955, **16**, 77
11 Natta, G., Corradini, P. and Bassi, I. W. *Nuvo Cimento, Suppl.* 1960, **15**, 68
12 Strobl, G. R. and Schneider, M. *J. Polym. Sci., Polym. Phys. Edn* 1980, **18**, 1343
13 Yano, O. and Wada, Y. *J. Polym. Sci. A2*, 1971, **9**, 669
14 Havriliak, S. and Negami, S. *Polymer* 1967, **8**, 161
15 Williams, M. L., Landel, R. E. and Ferry, J. D. *J. Am. Chem. Soc.* 1955, **77**, 3701
16 Boyd, R. H. and Aylwin, P. A. *Polymer* 1984, **25**, 330
17 Cook, M., Watts, D. C. and Williams, G. *Trans. Faraday Soc.* 1970, **66**, 2503
18 Williams, G. and Watts, D. C. *Trans. Faraday Soc.* 1970, **66**, 80

APPENDIX

When the values of the decay function in the long-time region are calculated by equation (4), the extrapolation to the lower frequency side is necessary. We show here

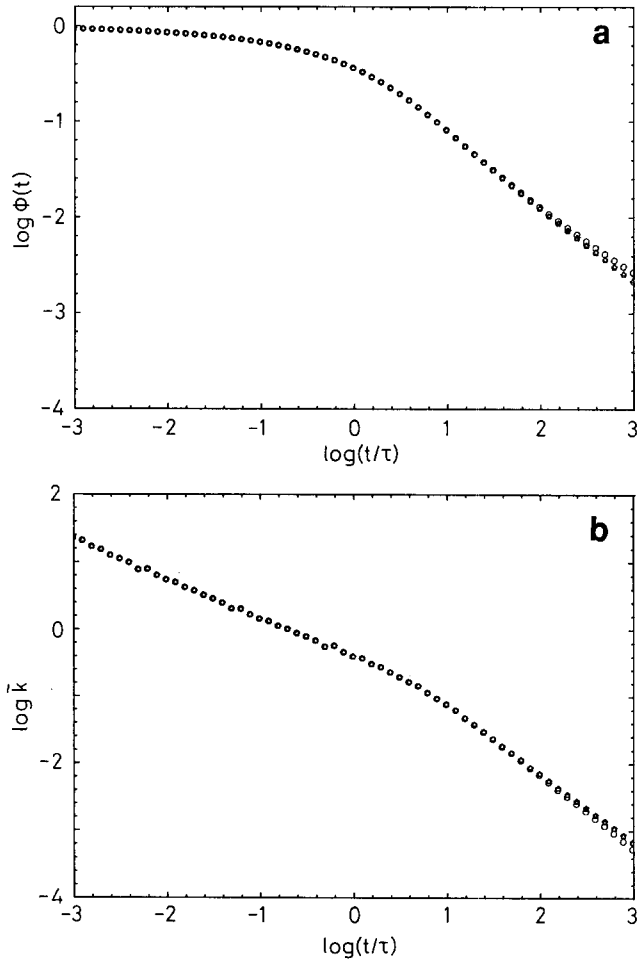

Figure 14 Variations in decay function and reduced rate constant caused by the extrapolation to the lower frequency side in $\varepsilon''/\varepsilon''_{max}$ *versus* f/f_{max} curves: △, power-law type; ⬠, Gaussian type with respect to $\log_{10}(f/f_{max})$; ○, Cauchy type with respect to $\log_{10}(f/f_{max})$. (a) Dependence of decay function on reduced time for iPS-6; (b) dependence of reduced rate constant on reduced time for iPS-6

that the calculated decay function in the time range shown in *Figure 11* hardly depends on the methods of extrapolation to the lower frequency side. Three kinds of extrapolation to the low frequency range are adopted beyond the experimental points.

1. Power-law type

$$\varepsilon''(\omega) = f_1\omega^{-n}$$

2. Gaussian type with respect to $\log_{10}\omega$

$$\varepsilon''(\omega) = g_0 \exp[-g_1 (\log_{10}\omega)^2]$$

3. Cauchy type with respect to $\log_{10}\omega$

$$\varepsilon''(\omega) = c_0/[1 + c_1(\log_{10}\omega)^2]$$

The sets of parameters (f_1, n), (g_0, g_1) and (c_0, c_1) are determined so that the extrapolation is connected smoothly with the experimental data points at low frequencies. As shown in *Figure 14a*, the variations in $\phi(t)$ with the types of extrapolation appear at t/τ larger than $10^{2.5}$ for iPS-6. The power-law decay region is observed regardless of the type of extrapolation. In cases 1 and 2 it is found that the power-law decay region exists in the range of $0.5 \leqslant \log(t/\tau) \leqslant 3$. Even in the case of 3, which corresponds to the extremely slow decay in the very-long-time region, it is found that the power-law region exists for more than two decades. It should be noted that the extrapolation to the high frequency region is not required to obtain the decay function in the long-time region. *Figure 14b* shows the dependence of the relaxation rate on t/τ. The crossover point from the WW equation to the power-law decay is independent of the choice of the low frequency tail.

From the above discussion, we conclude that the values of $\phi(t)$ are experimentally meaningful at least up to $10^{2.5}$ of t/τ.